SCIENCE CHINA
Earth Sciences

• RESEARCH PAPER •

June 2012 Vol.55 No.6: 949–965
doi: 10.1007/s11430-012-4372-9

Effects of melt percolation on the Re-Os systematics of continental mantle lithosphere: A case study of spinel peridotite xenoliths from Heilongjiang, NE China

YU SongYue[1*], SONG XieYan[1], XU YiGang[2], CHEN LieMeng[1] & LI Jie[2]

[1]*State Key Laboratory of Ore Deposit Geochemistry, Institute of Geochemistry, Chinese Academy of Sciences, Guiyang 550002, China;*
[2]*Key Laboratory of Isotope Geochronology and Geochemistry, Guangzhou Institute of Geochemistry, Chinese Academy of Sciences, Guangzhou 510640, China*

Received May 26, 2011; accepted January 16, 2012; published online March 8, 2012

Os isotope ratios of mantle peridotites have been considered to be largely immune to recent melt–rock interaction. However, Os isotope ratios and PGE (Platinum group elements) concentrations of the Yong'an xenoliths have been significantly modified by melt percolation, and are not suitable for determining the formation age of lithosphere mantle in Yong'an. In this study, the Yong'an spinel peridotite xenoliths are divided into two groups: N-Type and E-Type. The N-Type group including cpx (clinopyroxene)-poor lherzolite and harzburgite, shows a large variation of $Cr^{\#}$(sp) (13.2–48) and sulfur contents (from 171 ppm to below detection limit), whereas the E-Type peridotites are mainly refractory harzburgites and are characterized by high $Cr^{\#}$(sp) (35.3–42.2) and overall low sulfur contents (below 51 ppm). Both types show similar major and REE (rare earth element) patterns. Furthermore, the N-Type peridotites display a restricted range of iridium-group PGE (IPGE), Os/Ir and Ru/Ir ratios (Os/Ir = 0.64–1.12, Ru/Ir = 1.52–1.79) and variable palladium-group PGE (PPGE) contents (3.4–14.9 ppb), whereas the E-Type peridotites show a large variation of Os/Ir and Ru/Ir ratios (Os/Ir = 0.33–0.84, Ru/Ir = 0.94–1.6), and a restricted range of PPGE (4.3–6.9 ppb). $^{187}Os/^{188}Os$ ratios of E-Type peridotites are higher than those of N-Type peridotites at comparable fertility levels. These results suggest that N-Type peridotites may have been overprinted by metasomatism via small melt fractions, in which the percolation of the volatile-rich, small melt fractions only resulted in LILE (large ion lithophile element) enrichment of clinopyroxene, and their whole rock PGE contents and Re-Os isotope values were little changed. Moreover, E-Type peridotites may have been modified by melt-rock reaction involving relatively large melt fractions, which may result in the formation of secondary cpx and olivine and the removal of IPGE-bearing minerals such as Ru-Os-(Ir) alloys or laurite, followed by precipitation of secondary sulfides from melt with radiogenic isotopic signature.

peridotites, highly siderophile element, melt percolation, sulfides, NE China

Citation: Yu S Y, Song X Y, Xu Y G, et al. Effects of melt percolation on the Re-Os systematics of continental mantle lithosphere: A case study of spinel peridotite xenoliths from Heilongjiang, NE China. Sci China Earth Sci, 2012, 55: 949–965, doi: 10.1007/s11430-012-4372-9

During mantle melting, Re behaves as a mildly incompatible element, whereas Os behaves as a compatible element [1, 2]; consequently, most Os remains in the mantle and is much less affected than incompatible highly siderophile element (HSE, e.g., Re, Au, Pd) abundances by melt extraction. Moreover, Os isotope ratios of mantle peridotites have been considered to be largely immune to recent melt-rock interaction because of their high Os concentrations, in contrast to the extremely low Os abundances of basaltic melts [3, 4]. However, some recent studies of peridotite xenoliths have shown that Os and other HSE abundances can be greatly altered by small scale geological events such as

*Corresponding author (email: yusongyuegyig@hotmail.com)

metasomatic and melt percolation processes; consequently, Os model age results cannot be related to particular crustal formation events [5–11].

Studies of Re-Os systematics of peridotite xenoliths hosted by Cenozoic basalts from NE China (including the Hinggan-Mongolian Orogenic Belt and North China Craton) have yielded evidence that in this region, most samples have young T_{RD} (Re depletion age, <1.0 Ga) ages and define no or, at best, very poor correlation between $^{187}Os/^{188}Os$ and indicators of melt depletion (such as spinel $Cr^{\#}$ or whole rock Al_2O_3 contents). The young model ages, particularly for the highly refractory peridotite from eastern China, are considered to be related to recent melt extraction, so the Os isotopic composition has not had enough time to evolve to match Re/Os ratio [4, 12, 13]. Nevertheless, Zhang et al. [14] argued that Re-Os isotopic ages of the mantle xenoliths hosted by Cenozoic basalts reflect the result of peridotite-melt interaction, rather than the true formation age of the lithospheric mantle. Moreover, study of the Re-Os systematics of the peridotite xenoliths from east central China has provided evidence that Re-Os concentrations and isotope ratios of the mantle peridotites have clearly been modified by melt percolation [15]. Therefore, whether and to what extent the Re-Os systematics of peridotite xenoliths from NE China has been affected by interaction with melts or fluids is not well understood. The nature of the metasomatic melts or fluids responsible for modifying the Re-Os systematics of the mantle peridotites also remains poorly constrained.

In this work, PGE concentrations and Re-Os isotopic compositions of peridotite xenoliths from Yong'an, Heilongjiang province, were used to investigate the effects of melt-peridotite interaction. The results show that Os isotope ratios and PGE concentrations of Yong'an xenoliths have been modified by melt percolation, and are therefore not reliable in constraining the formation age of mantle lithosphere beneath Yong'an.

1 Geological setting and sample descriptions

Hinggan-Mongolian Orogenic Belt (HMOB) in NE China (Figure 1(a)) is a composite fold belt formed by amalgamation of several minor blocks during subduction and collision between the Siberian and North China Craton [16]. Widespread A-type granites in the HMOB are characterized by low initial Sr ratios, positive $\varepsilon_{Nd}(t)$ values, and mainly young T_{DM} Nd isotopic model ages (0.89±0.22 Ga) [4]. Since the late Mesozoic, HMOB became an important part of the circum-Pacific tectonic-magmatic zone. During the Cenozoic, extensive eruption of basalts occurred along the Yi-Shu and Dun-Mi faults [17]. Some of these basalts (most are Neogene and Quaternary alkaline basalts) contain ultramafic mantle-derived xenoliths.

The peridotite xenoliths studied in this paper were collected from Yong'an (Figure 1(b)), Heilongjiang Province. The host lavas vary from basanite to tholeiitic basalt, with Ar-Ar ages ranging from 31.96 to 13.4 Ma [18]. Xenoliths are hosted mainly by basanite, and are fresh (L.O.I <0.3%) and large (with maximum diameters of over 50 cm). Peridotites from this region are similar to Group I peridotites [19], characterized by porphyroclastic textures with fine- to medium-grainsize and occasional porphyroblasts of orthopyroxene (Figure 2(a)). Volatile-bearing accessory minerals such as amphibole and phlogopite are not observed, and

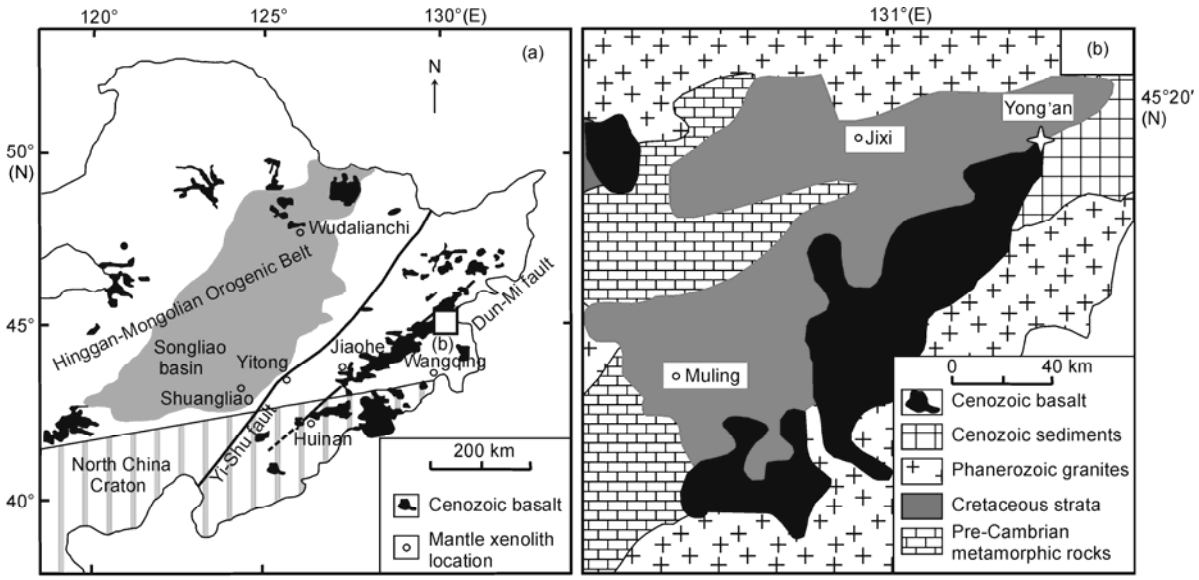

Figure 1 Sketch map showing the simplified tectonic framework of NE China and location of the studied area (a) and enlarged map of the studied area (b). The samples in this study were collected from Yong'an. Yi-Shu fault and Dun-Mi fault represent Yilan-Shulan fault zone and Dunhua-Mishan fault zone respectively.

some orthopyroxene grains are replaced by clinopyroxene and olivine adjacent to pockets of silicate glass (Figure 2(b)), which may represent the residual liquid after melt-peridotite interaction. This reaction texture is also documented in Shuangliao peridotite xenoliths [20].

Sulfides were examined microscopically in detail. There is no significant difference in the sulfide petrographic features or sulfur contents between these two types of Yong'an peridotites. Fertile samples (e.g., YA-2) contain slightly more sulfides, whereas refractory harzburgites are very poor in, or lack sulfides. Sulfide grains are generally small (<5 μm in diameter) and interstitial, although some are enclosed in silicate minerals (Figure 2(c) and (d)); Table 1). Cu-rich vein sulfides are also present along cracks in olivine crystals (Figure 2(c)). In all samples, the sulfides are dominantly pentlandite and millerite (Table 1). Secondary Cu-rich sulfides are rare.

2 Sample preparation and analytical methods

The xenoliths for this study were cut to remove exterior

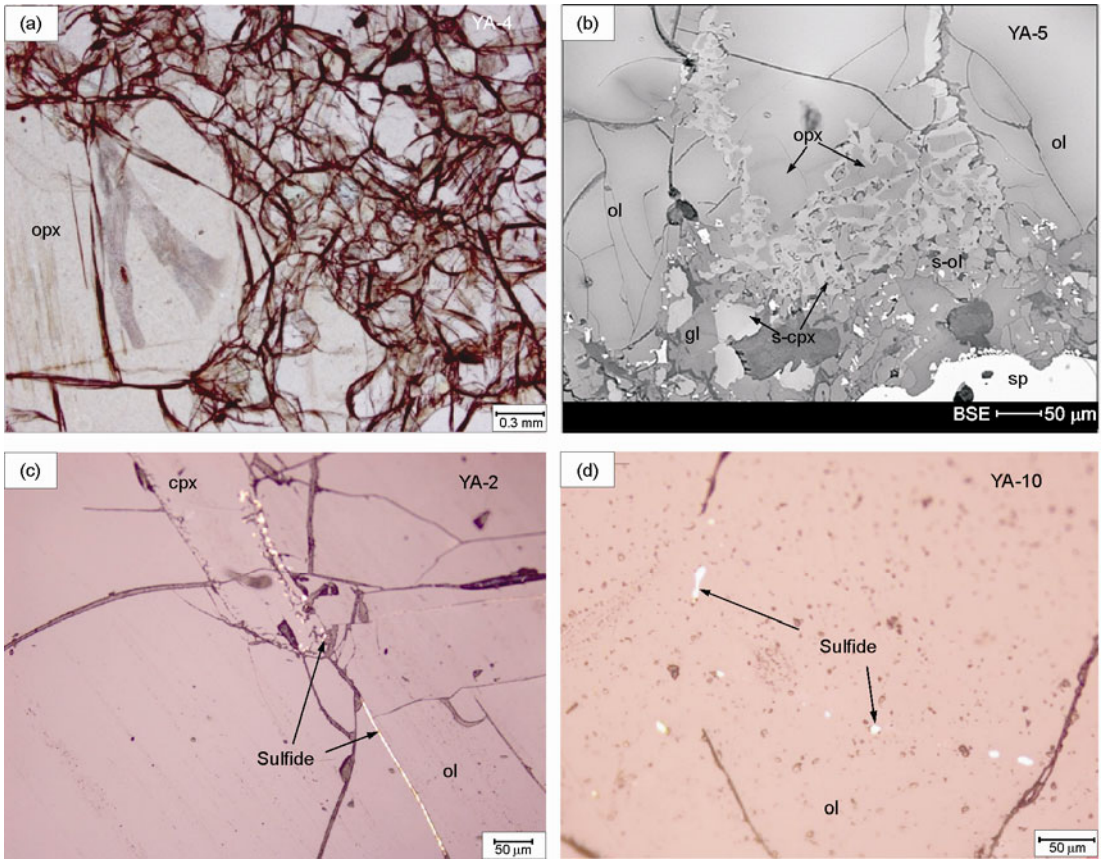

Figure 2 Photomicrograph showing textures in Yong'an peridotite xenoliths. (a) Porphyroclastic texture with orthopyroxene (opx) as porphyroclast; (b) primary orthopyroxene rimmed by secondary clinopyroxene (s-cpx) and secondary olivine (s-ol), with adjacent silicate glasses (gl); (c) interstitial sulfides as droplet or vein, located on grain boundaries or along cracks in olivine crystals; (d) sulfides included in olivine.

Table 1 Major element compositions (%) of representative sulfides in Yong'an peridotite[a)]

Sample	N-Type									E-Type			
	YA-2					YA-5	YA-9			YA-7	YA-10		
Assemblage	Pn	Ml	Pn	Pn	Cu-rich Pn	Cu-rich Pn	Pn	Pn	Pn	Pn	Cu-rich Pn	Pn	Cu-rich Pn
Type	inter	inter	inter	inter	inter	in	inter	inter	inter	inter	in	in	in
S	32.92	27.85	33.20	33.09	33.19	34.67	31.48	32.09	30.75	41.96	31.95	33.01	31.85
Fe	30.24	4.41	27.30	31.40	26.47	36.28	26.84	27.46	27.60	32.46	28.49	32.65	31.34
Co	0.40	0.00	0.37	0.37	0.28	0.40	0.58	0.59	0.60	0.35	0.36	0.34	0.34
Ni	33.84	69.70	38.95	33.13	32.85	25.15	39.70	40.41	39.46	25.43	32.94	33.15	33.93
Cu	0.40	0.01	0.01	0.22	5.84	1.69	0.01	0.03	0.01	0.16	4.41	0.10	1.90
Total	97.81	101.97	99.83	98.21	98.63	98.19	98.61	100.58	98.42	100.36	98.14	99.26	99.36

a) inter = interstitial; in = inclusion; Pn = Pentlandite; Ml = Millerite.

surfaces. Relatively fresh interiors without basaltic veins were used for bulk-rock analyses and for mineral separation. The rocks were crushed in a steel mortar and ground in a steel mill. Chemical analyses were performed at the Institute of Geochemistry, Chinese Academy of Sciences (IGCAS). Major elements were measured by X-ray fluorescence. The rocks were also analyzed for trace elements abundances using an Inductively Coupled Plasma-Mass Spectrometer (ICP-MS), following the analytical procedures described by Qi et al. [21]. The analytical precision for most minor and trace elements is better than ±5%.

PGE analyses were done by ID-ICP-MS at Institute of Geochemistry, Chinese Academy of Sciences (IGCAS). Fifteen grams of powdered samples were digested with HF and aqua regia combined with a sodium peroxide fusion and Te co-precipitation. A detailed description of the method for the PGE is presented by Qi et al. [22]. Precision and accuracy are demonstrated by analyzing reference materials, including WGB-1 (Gabbro) and TDB-1 (Diabase), and are shown in Table 2. The concentrations determined for Ir, Ru and Rh in WGB-1 and TDB-1 are lower than the recommended values, but agree well with values reported by Meisel and Moser [23]. The procedural blank for all PGE is generally <0.4 ppb; their contributions are negligible because most samples have concentrations that are at least 20 times higher.

Re-Os analyses were carried out at Guangzhou Institute of Geochemistry, Chinese Academy of Sciences (GIGCAS). The chemical separation techniques for Re-Os analyses employed in this study have followed previously published work [25–28]. In brief, Os and Re concentrations and Os isotopic measurements were made on bulk samples using 1–2 g of powder. Samples were spiked with solutions enriched in ^{190}Os and ^{185}Re and digested in inverse aqua regia in sealed Carius tubes at 240°C for at least 24 hours [25]. Osmium was extracted by carbon tetrachloride and subsequently back-extracted into high-purity concentrated HBr [26, 27]. Further purification of Os was accomplished via micro-distillation in a conical Teflon vial [29]. The purified Os was at this stage ready for mass spectrometry. The Re-bearing solution was then evaporated to reduce the volume of the solution, and diluted with water. Subsequently, the solution was centrifuged to remove the residual precipitate. Rhenium was then separated from the aqueous phase using Bio-Rad AG 1-X8 anion exchange resin (100–200 mesh).

The isotopic compositions of Os were measured using negative thermal ionization mass spectrometry (Thermo-Finnigan Triton). The mass spectrometric procedures followed in this study have been discussed in Creaser et al. [30] and Volkening et al. [31]. The Os was loaded onto high purity Pt filament (99.999%, 1 mm × 0.025 mm, H. Cross Co. Ltd.) that had been previously baked in air to a bright red temperature for more than 3 minutes. The sample was covered with 10 μg Ba using a custom-made 10000 ppm $Ba(NO_3)_2$ solution (CLARITAS, SPEX Inc.). Osmium isotopic compositions were measured in pulse-counting electron multiplier mode. Instrumental mass fractionation of Os was corrected for by normalizing the measured ^{192}Os/^{188}Os ratio to 3.08271 [32]. Oxide corrections were made using ^{17}O/^{16}O = 0.00037 and ^{18}O/^{16}O = 0.002047. Rhenium was determined by ICP-MS (PerkinElmer, Elan 6000). The total blank levels for Re and Os were 2–5 and 3–6 pg, respectively, and are negligible compared to their concentrations in most samples. All data were corrected for blanks and the isotopic and concentration data.

Sulfur analyses were determined using high temperature combustion combined with infrared spectrometry using a Horiba 220V S-C analyzer at the University of Quebec, Chicoutimi. The protocol outlined in Bédard et al. [33]. The detection limit is 31 ppm.

3 Results

3.1 Mineral compositions

Modal compositions of the studied xenoliths were calculated by a least-square fit method using constituent mineral chemistry and bulk geochemistry. In diagrams of $Cr^{\#}$(sp) versus $Mg^{\#}$ and TiO_2 contents in minerals, some samples show significant Fe and Ti enrichment compared to the partial melting trend (Figure 3, Table 3). For convenience in description, these samples are referred to as E-Type xenoliths. Samples plot on the partial melting trend are referred to as N-Type xenoliths. The N-Type group including cpx (clinopyroxene)-poor lherzolite and harzburgite, shows a large variation of $Cr^{\#}$(sp) (13.2–48, Table 3). The typical

Table 2 Blank (ng), detection limits (ppb) and analytical results (ppb) for reference materials, WGB-1 and TDB-1[a)]

	Blank	WGB-1 (gabbro)			TDB-1 (dolerite)		
		Certified	Meisel	This study	Certified	Meisel	This study
Ir	0.02	0.33	0.211	0.20	0.15	0.075	0.10
Ru	0.06	0.3	0.144	0.11	0.3	0.198	0.26
Rh	0.02	0.32	0.234	0.21	0.7	0.471	0.44
Pt	0.22	6.1	6.39	4.78	5.8	5.01	4.54
Pd	0.32	13.9	13.9	14.72	22.4	24.3	21.80

a) Data of "Meisel" is from ref. [23], data of "Certified" is from ref. [24].

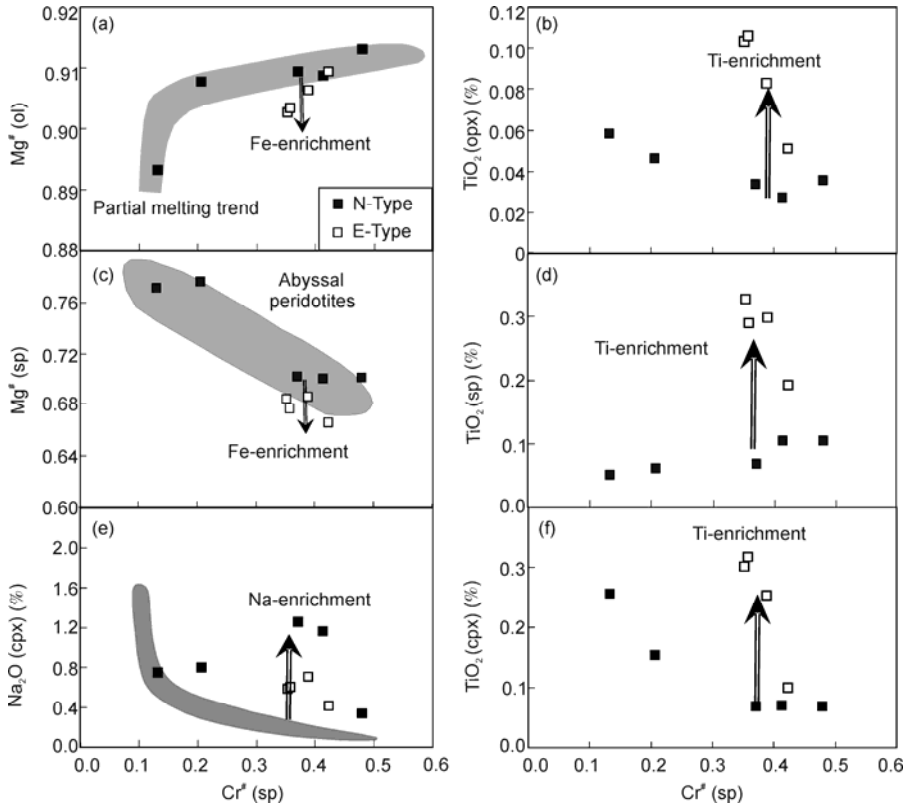

Figure 3 Diagrams illustrating concentrations of selected elements in different minerals of Yong'an peridotites. (a) Correlation of Fo versus $Cr^{\#}$ (Cr/(Cr+Al)) of spinel in Yong'an peridotites, the partial melting trend is from ref. [34]; (b) TiO_2 content in orthopyroxene versus $Cr^{\#}$ of spinel; (c) $Mg^{\#}$ versus $Cr^{\#}$ of spinel, abyssal peridotite trend is after ref. [35]; (d) TiO_2 content versus $Cr^{\#}$ in spinel; (e) Na_2O content in clinopyroxene versus $Cr^{\#}$ of spinel; (f) TiO_2 content in clinopyroxene versus $Cr^{\#}$ in spinel. The partial melting trend is modeled by melting a fertile source rock with 0.13 % TiO_2, using the fractional melting model of ref. [36].

mineral assemblage (Table 4) is olivine (ol, 64.3%–79.3%), orthopyroxene (opx, 16.5%–20.6%), clinopyroxene (cpx, 3.5%–11.9%) and spinel (sp, 1.7%–2.7%); whereas the E-Type peridotites are mainly refractory harzburgites, and characterized by high $Cr^{\#}$(sp) (35.3–42.2), The typical mineral assemblage is olivine (73.6%–81.8%), orthopyroxene (16.1%–21.2%), clinopyroxene (2.4%–4.8%) and spinel (0.8%–1.6%). It is worth noting that samples in both types plot above the partial melting trend in $Cr^{\#}$(sp) versus Na_2O(cpx) diagram (Figure 3(e)). Equilibrium temperatures were estimated using the two-pyroxene thermometers of Bertrand and Mercier [37] and Wells [38] and the empirical thermometer of Witt-Eickschen and Seck [39] based on Cr-Al exchange between opx and spinel (Table 4). For a given sample, these three thermometers yield similar estimates, consistent with the homogeneous mineral compositions. N-Type samples show relatively high and variable equilibrium temperature (918–998°C, using the thermometer of Wells [38], whereas E-Type samples tend to have lower, more homogeneous equilibrium temperatures (911–928°C).

3.2 Trace elements of separated clinopyroxenes

Cpx in Yong'an peridotites exhibits substantial variations in both concentrations of trace elements (Table 5) and chondrite-normalized REE patterns (Figure 4(a)–(d)). Cpx from N-Type peridotites is either selectively enriched in LREE with a flat MREE-HREE pattern (e.g., YA-2 and YA-9) or enriched in LREE and MREE with a relatively flat HREE pattern (e.g., YA-5 and YA-8). LREE enrichment of cpx in the N-Type peridotites is coupled with positive Th, U and Sr anomalies and negative high field strength element (HFSE) anomalies (including Nb, Ta, Zr, Hf). HFSE abundances in cpx from N-Type peridotites display contrasting geochemical behavior; for example, Nb and Ta contents are low and homogeneous, whereas Zr and Hf contents are generally high and variable (Table 5, Figure 4(b)), displaying positive correlation with La/Yb (not shown). In contrast to the variable LREE enrichment of cpx from N-type peridotites ($(La/Yb)_n$ varying from 1.2 to 11.2), cpx from E-Type peridotites display relatively flat and homogeneous REE patterns ($(La/Yb)_n$ varying from 1.7 to 2.8), relatively weak positive Th, U and Sr anomalies, and negative high field strength element (HFSE) anomalies (Figure 4(c–d)).

3.3 Whole rock major elements compositions

As shown in Table 4 and Figure 5(a)–(d), the MgO content

Table 3 Mineral composition (%) of mantle xenoliths from Yong'an

Sample	N-Type															
	YA-1				YA-2				YA-3				YA-5			
Assemblagee	ol	opx	cpx	sp	ol	opx	cpx	sp	ol	opx	cpx	sp	ol	opx	cpx	sp
Na_2O	0.00	0.00	0.34	0.04	0.00	0.03	0.76	0.00	0.01	0.09	1.26	0.00	0.00	0.09	0.96	0.01
SiO_2	40.72	56.86	54.73	0.02	39.66	55.87	53.77	0.00	40.58	57.09	54.15	0.02	40.95	56.00	54.56	0.04
MgO	49.19	33.61	17.43	15.59	47.87	32.80	15.96	19.19	48.97	33.41	16.59	16.24	48.80	33.45	16.69	15.20
MnO	0.11	0.11	0.08	0.14	0.14	0.15	0.10	0.09	0.10	0.11	0.09	0.16	0.12	0.12	0.05	0.19
TiO_2	0.00	0.04	0.07	0.11	0.01	0.06	0.26	0.05	0.01	0.03	0.07	0.07	0.00	0.03	0.07	0.08
Al_2O_3	0.00	1.73	1.88	29.13	0.00	3.49	3.71	56.95	0.01	2.49	2.48	37.36	0.00	2.09	2.58	33.17
CaO	0.03	0.66	22.41	0.00	0.04	0.64	22.25	0.00	0.03	0.63	20.99	0.01	0.14	0.57	22.10	0.01
NiO	0.37	0.08	0.03	0.18	0.31	0.07	0.03	0.33	0.39	0.07	0.04	0.17	0.36	0.08	0.03	0.16
FeO	8.43	5.37	2.01	11.93	10.29	6.51	2.41	10.21	8.77	5.51	2.22	12.41	8.85	5.58	2.30	12.15
Cr_2O_3	0.01	0.41	0.58	39.99	0.02	0.29	0.49	12.93	0.01	0.50	0.89	32.74	0.05	0.49	0.75	36.58
Total	98.86	98.87	99.55	97.11	98.33	99.91	99.73	99.76	98.87	99.92	98.78	99.19	99.20	98.50	98.83	98.95
$Mg^{\#}$	91.2	91.8	93.9	70.0	89.2	90.0	92.2	77.0	90.9	91.5	93.0	70.0	90.8	91.4	92.8	69.0
$Cr^{\#}$		13.7	17.2	48.0		5.3	8.1	13.2		11.9	19.4	37.0	100.0	13.7	16.4	42.5

Sample	N-Type												E-Type			
	YA-5				YA-8				YA-9				YA-4			
Assemblage	glass-1	glass-2	glass-3	glass-4	ol	opx	cpx	sp	ol	opx	cpx	sp	ol	opx	cpx	sp
Na_2O	4.57	7.29	6.34	0.05	0.00	0.07	1.16	0.00	0.00	0.02	0.81	0.00	0.01	0.02	0.42	0.01
SiO_2	65.26	59.70	66.63	0.93	40.31	56.57	54.78	0.00	41.01	55.56	53.95	0.02	40.22	57.14	54.20	0.00
MgO	0.03	0.16	0.01	0.70	49.15	34.07	16.32	15.81	48.96	32.88	16.15	18.64	48.71	33.76	17.21	14.88
MnO	0.00	0.01	0.02	0.00	0.12	0.12	0.06	0.20	0.12	0.13	0.08	0.12	0.12	0.13	0.08	0.20
TiO_2	0.13	0.10	0.19	0.01	0.00	0.03	0.07	0.10	0.01	0.05	0.15	0.06	0.01	0.05	0.10	0.19
Al_2O_3	19.02	25.04	20.94	0.30	0.00	2.26	2.78	34.10	0.01	3.29	3.87	50.39	0.00	1.91	2.04	33.17
CaO	0.00	5.42	0.81	44.49	0.06	0.56	21.63	0.00	0.06	0.59	22.24	0.01	0.03	0.66	23.04	0.01
NiO	0.02	0.02	0.01	0.00	0.36	0.08	0.05	0.10	0.36	0.06	0.03	0.27	0.37	0.07	0.05	0.15
FeO	0.21	0.23	0.19	0.30	8.88	5.28	2.04	12.18	8.95	5.45	2.24	9.65	8.74	5.62	2.12	13.44
Cr_2O_3	0.00	0.06	0.02	0.01	0.04	0.42	0.85	35.76	0.01	0.41	0.66	19.52	0.02	0.41	0.55	36.12
K_2O	0.17	0.03	0.22	0.09												
Total	89.41	98.05	95.36	46.87	98.92	99.47	99.75	98.27	99.49	98.44	100.17	98.67	98.24	99.77	99.81	98.17
$Mg^{\#}$	21.7	54.8	4.5	80.9	90.8	92.0	93.4	69.8	90.7	91.5	92.8	77.5	90.9	91.5	93.5	66.4
$Cr^{\#}$						11.1	17.1	41.3		7.7	10.2	20.6		12.6	15.4	42.2

(*To be continued on the next page*)

(*Continued*)

Sample	E-Type											
	YA-6				YA-7				YA-10			
Asseblage	ol	opx	cpx	sp	ol	opx	cpx	sp	ol	opx	cpx	sp
Na_2O	0.01	0.01	0.59	0.00	0.00	0.01	0.60	0.00	0.00	0.02	0.71	0.00
SiO_2	39.80	56.48	53.70	0.03	40.60	56.03	54.50	0.05	40.69	56.10	54.22	0.00
MgO	49.16	33.56	16.61	15.90	48.83	33.81	16.69	15.66	48.62	33.72	16.38	15.78
MnO	0.14	0.13	0.06	0.18	0.14	0.13	0.07	0.18	0.11	0.12	0.08	0.19
TiO_2	0.02	0.10	0.30	0.33	0.00	0.11	0.32	0.29	0.01	0.08	0.25	0.30
Al_2O_3	0.00	2.34	3.00	37.57	0.00	2.31	2.42	38.07	0.00	2.28	2.89	35.15
CaO	0.04	0.61	22.83	0.00	0.03	0.58	22.81	0.00	0.04	0.66	22.13	0.03
NiO	0.36	0.09	0.04	0.20	0.33	0.08	0.03	0.19	0.37	0.07	0.03	0.14
FeO	9.54	5.89	2.28	13.21	9.40	5.77	2.36	13.45	9.05	5.61	2.26	13.01
Cr_2O_3	0.01	0.41	0.69	30.49	0.02	0.43	0.54	31.53	0.01	0.45	0.81	33.24
Total	99.07	99.61	100.11	97.92	99.36	99.25	100.34	99.42	98.89	99.11	99.75	97.83
$Mg^{\#}$	90.2	91.0	92.9	68.2	90.3	91.3	92.6	67.5	90.5	91.5	92.8	68.4
$Cr^{\#}$		10.6	13.4	35.3		11.2	13.0	35.7		11.7	15.9	38.8

Table 4 Modal compositions, equilibrium temperatures, major element compositions and Re-Os isotope and PGE data of Yong'an xenoliths[a)]

Sample	N-Type						E-Type			
	YA-1	YA-2	YA-3	YA-5	YA-8	YA-9	YA-4	YA-6	YA-7	YA-10
Modes (%)										
ol	77.1	64.3	79.3	76.7	78.7	73.5	81.8	73.6	77.4	81.2
opx	18.6	20.6	16.5	19.2	17.3	17.0	16.1	21.2	17.9	16.2
cpx	3.5	11.9	4.2	3.9	4.2	8.3	2.9	4.8	4.3	2.4
sp	1.8	2.6	1.9	2.7	1.7	2.3	1.6	1.6	1.6	0.8
Equilibrium temperatures (°C)										
BM85	963	877	919	870	895	890	861	848	856	913
W77	998	929	952	923	928	937	923	911	918	920
WS	861	890	929	913	891	928	868	883	891	898
Major element compositions (%)										
SiO_2	44.25	43.96	43.76	43.73	43.59	43.94	43.55	43.73	43.68	43.36
MgO	45.58	40.73	45.31	44.79	45.49	43.28	46.01	44.32	44.81	45.42
TiO_2	0.00	0.04	0.00	0.02	0.00	0.01	0.01	0.04	0.03	0.01
Al_2O_3	0.96	2.78	1.15	1.26	1.04	1.94	0.90	1.19	1.08	0.69
Fe_2O_3	7.98	9.05	8.43	8.56	8.04	8.30	8.48	8.87	8.96	9.11
MnO	0.11	0.12	0.11	0.12	0.11	0.11	0.11	0.12	0.12	0.11
CaO	0.77	2.66	0.84	0.85	0.83	1.84	0.64	1.11	0.98	0.62
Na_2O	0.00	0.06	0.00	0.00	0.00	0.00	0.00	0.00	0.00	0.00
P_2O_5	0.00	0.01	0.01	0.01	0.02	0.01	0.01	0.01	0.01	0.03
Total	99.66	99.39	99.60	99.33	99.12	99.43	99.70	99.38	99.67	99.35
LOI	0.00	0.10	0.01	0.23	0.26	0.22	0.12	0.14	-0.04	0.27
Sulfur (ppm), PGEs (ppb) and Re-Os isotope compositions										
Sulfur	171			<31	<31	75	39	51	<31	<31
Ir	4.12			3.79	4.45	4.17	2.93	1.88	1.72	3.37
Ru	6.26			5.87	7.95	6.71	4.16	1.76	1.83	5.39
Rh	1.34			0.87	1.16	1.25	0.80	0.67	0.76	0.81
Pt	7.90			2.21	4.42	6.77	2.86	2.86	2.89	4.10
Pd	7.00			1.14	1.53	5.50	0.68	2.86	3.25	1.71
Re	0.13			0.20	0.05	0.21	0.13	0.02	0.10	0.20
Os	4.17			2.87	2.85	4.68	2.09	1.00	0.57	2.83
Os/Ir	1.01			0.76	0.64	1.12	0.72	0.53	0.33	0.84
Ru/Ir	1.52			1.55	1.79	1.61	1.42	0.94	1.06	1.60
$^{187}Re/^{188}Os$	0.145			0.335	0.076	0.214	0.308	0.099	0.876	0.337
$^{187}Os/^{188}Os$	0.12264±84			0.11179±41	0.11436±92	0.12110±39	0.11749±38	0.12752±39	0.12105±89	0.12189±46
T_{RD} (Ga)	0.65			2.23	1.86	0.87	1.40	future	0.88	0.76

a) Modal compositions are calculated from bulk compositions and constituent mineral chemistries using least-squares regression method. Thermometers: BM85: two-pyroxene thermometer of Bertrand and Mercier [37]; W77: two-pyroxene thermometer of Wells [38]; WS: Cr-Al-opx thermometer of Witt-Eickschen and Seck [39]; Pressure of 1.5 GPa assumed throughout. T_{RD}: Re depletion age, the parameters used in the calculation are λ_{Re}=1.666×10^{-11}/yr, $(^{187}Re/^{188}Os)_{Chond}$=0.40186 and $(^{187}Os/^{188}Os)_{Chond,0}$=0.1270 [40].

of the most refractory sample (YA-2) is 46%, and Al_2O_3 and CaO contents in this sample are low (0.9% and 0.64%, respectively). The most fertile sample (YA-2) is still compositionally more depleted than the primitive mantle [44] and has Al_2O_3 and CaO contents of 2.78% and 2.66%, respectively. For N-Type peridotites, Al_2O_3, CaO and TiO_2 are negatively correlated with MgO (Figure 5) and show trends similar to those observed for xenoliths from Shuangliao, Jiaohe, and other spinel lherzolite localities worldwide, which have been interpreted as residues of variable degrees of partial melting [42, 45, 46]. For E-Type peridotites, Al_2O_3 and CaO are also negatively correlated with MgO, but they display slightly higher TiO_2 and FeO at comparable MgO, compared to the usual depletion trend (Figure 5(b) and (d)).

3.4 PGE and Re-Os isotopic compositions in whole rock

As shown in Table 4, with the exception of YA-2, most analyzed samples are strongly depleted in sulfur (⩽75 ppm) compared to primitive upper mantle (250 ppm) [47], in agreement with petrographic observations. There is no distinction of sulfur abundances between N-Type and E-Type peridotites.

Total PGE contents of Yong'an xenoliths (Table 4) are generally lower than those in Pyrenean orogenic lherzolites [48]. The N-Type peridotites show significantly higher and

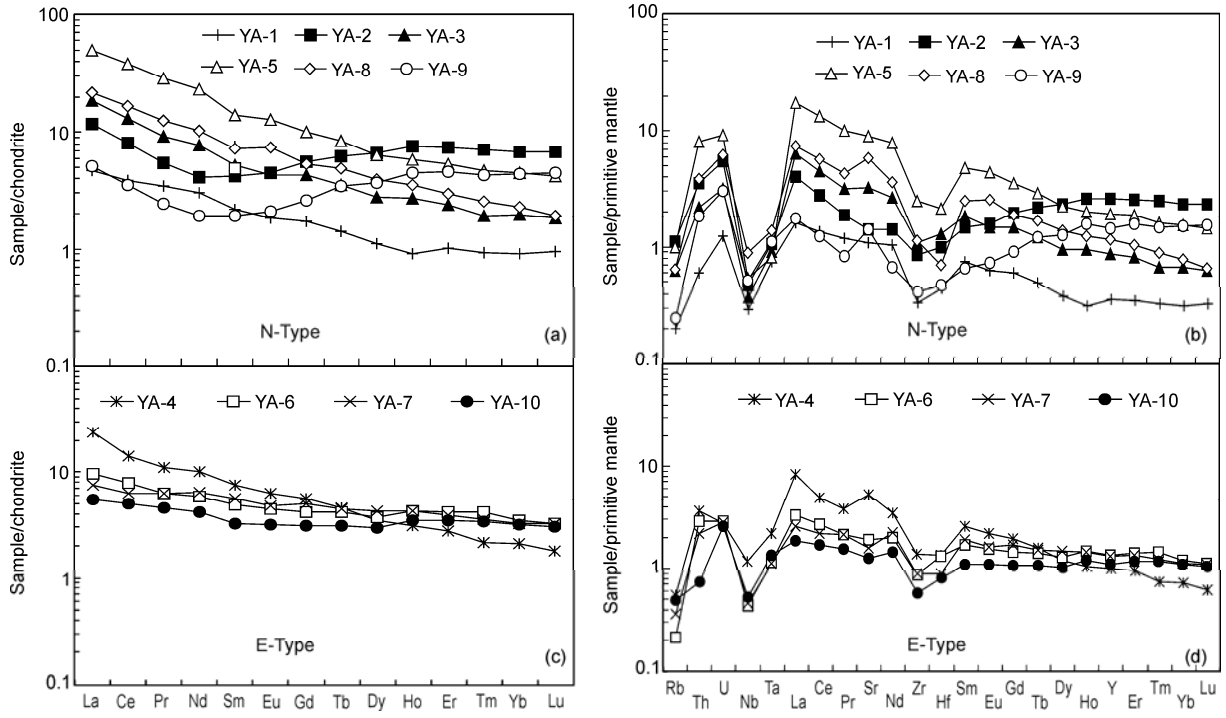

Figure 4 REE and trace element abundances of clinopyroxene from Yong'an peridotites. Normalization values are from ref. [41].

Table 5 Trace element concentration (ppm) in clinopyroxenes from Yong'an xenoliths

Sample	N-Type						E-Type			
	YA-1	YA-2	YA-3	YA-5	YA-8	YA-9	YA-4	YA-6	YA-7	YA-10
Sc	48.9	55.8	48.1	63.0	50.9	52.7	54.8	59.2	53.2	61.5
V	137	219	140	195	142	195	149	153	143	153
Cr	3145	2894	4182	4810	4182	3463	4048	3639	3329	4140
Co	38.6	39.6	56.6	56.3	63.2	55.2	51.3	56.0	62.7	57.4
Ni	715	772	1050	1020	1160	1020	972	980	1090	1040
Pb	0.33	0.50	0.59	0.45	1.26	0.31	0.62	0.17	0.05	0.01
Cu	5.83	29.8	15.9	17.9	5.59	16.1	16.3	14.1	5.64	34.9
Yb	0.15	1.16	0.33	0.76	0.39	0.75	0.36	0.59	0.55	0.54
Rb	0.13	0.71	0.40	0.63	0.41	0.16	0.35	0.14	0.23	0.31
Th	0.05	0.30	0.19	0.69	0.33	0.16	0.31	0.25	0.19	0.06
U	0.03	0.11	0.07	0.20	0.13	0.06	0.06	0.06	0.06	0.05
Nb	0.21	0.34	0.26	0.38	0.63	0.37	0.83	0.31	0.33	0.37
Ta	0.03	0.04	0.04	0.03	0.06	0.05	0.09	0.05	0.05	0.06
La	1.11	2.79	4.39	11.9	5.14	1.21	5.67	2.30	1.76	1.29
Ce	2.38	4.97	8.02	23.5	10.1	2.17	8.75	4.77	3.86	3.03
Pr	0.33	0.52	0.88	2.76	1.18	0.23	1.06	0.59	0.59	0.43
Sr	23	29	68	191	124	30	112	40	33	27
Nd	1.40	1.91	3.60	10.8	4.83	0.90	4.74	2.73	3.00	1.96
Zr	3.71	9.46	12.1	28.0	12.8	4.61	15.5	9.83	9.87	6.44
Hf	0.14	0.31	0.40	0.66	0.22	0.15	0.42	0.41	0.27	0.25
Sm	0.33	0.65	0.81	2.14	1.11	0.29	1.15	0.75	0.85	0.49
Eu	0.11	0.26	0.25	0.74	0.43	0.12	0.37	0.26	0.28	0.18
Gd	0.36	1.16	0.88	2.09	1.11	0.54	1.16	0.86	1.02	0.64
Tb	0.05	0.24	0.13	0.32	0.18	0.13	0.17	0.15	0.17	0.12
Dy	0.28	1.70	0.70	1.63	1.01	0.93	0.89	0.95	1.09	0.76
Ho	0.05	0.43	0.16	0.33	0.20	0.26	0.17	0.24	0.24	0.20
Y	1.63	11.8	3.95	8.68	5.27	6.60	4.58	6.16	6.01	4.99
Er	0.17	1.23	0.39	0.89	0.49	0.76	0.46	0.68	0.64	0.57
Tm	0.02	0.18	0.05	0.12	0.07	0.11	0.05	0.11	0.09	0.09
Lu	0.02	0.17	0.05	0.11	0.05	0.11	0.05	0.08	0.08	0.08

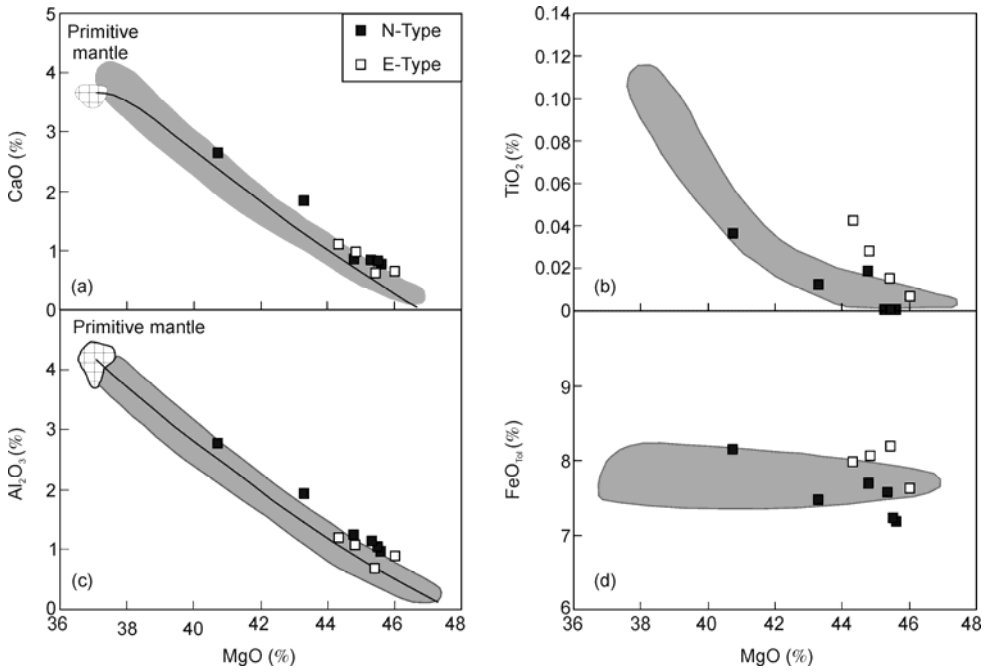

Figure 5 Plots of CaO, TiO_2, Al_2O_3, FeO against MgO for peridotite xenoliths from Yong'an. The shaded fields represent the compositional range for worldwide peridotites [42]. Black line is near-fractional melting model trend of a starting source of primitive spinel peridotite using the model of Niu [43]; Primitive mantle compositions are after ref. [44].

more variable total PGE contents (13.9–26.6 ppb) than the E-Type samples (10–15.4 ppb). In addition, the N-Type peridotites show a relatively restricted range of IPGE contents (12.5–15.6 ppb) combined with a wide range of PPGE content (4.2–16.2 ppb). In contrast, the E-Type peridotites have variable IPGE contents, increasing from 4.1 ppb in YA-7 to 11.6 ppb in YA-10, with a restricted range of PPGE (4.3–6.9 ppb). As shown in (Figure 6(a)), two N-Type peridotites (YA-2, YA-9) display flat PGE patterns normalized to Chondrite values, similar to primitive mantle [49]. The other N-Type peridotites (YA-5, YA-8) have flat IPGE patterns and are depleted in PPGE relative to IPGE. These patterns are similar to those from other peridotite xenoliths and massifs worldwide [10, 48, 51–53]. Nevertheless, a humped PGE pattern with a peak at Ir is observed in the some E-Type samples (e.g., YA-4). Some other E-Type peridotites (e.g., YA-6, YA-7) have a large variation in PGE concentrations (Figure 6(b)).

Measured Os concentrations of all Yong'an samples range from 0.57 to 4.68 ppb and Re concentrations vary from 0.02 to 0.21 ppb (Table 4). Whole rock $^{187}Os/^{188}Os$ isotopic compositions of Yong'an peridotite xenoliths range from 0.11179 to 0.12752.

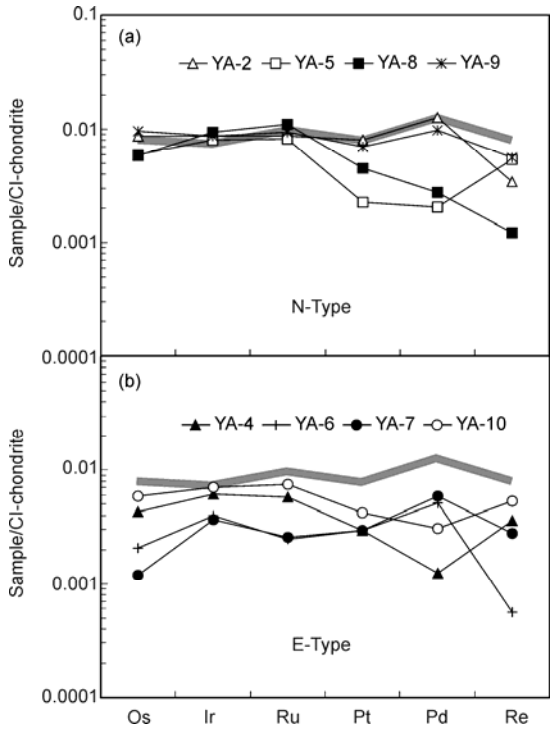

Figure 6 Diagrams of highly siderophile element (HSE) patterns of N-Type and E-Type samples from Yong'an. Grey solid line represents primitive upper mantle (PUM) composition [49]. Chondrite normalizing values are after ref. [50].

4 Discussion

As described above, the Yong'an N-Type and E-Type peridotites are distinctive, not only in major and trace element compositions of olivine, clinopyroxene and spinel (Figures 3 and 4) but also in whole rock PGE and Re-Os isotopic compositions (Table 4). Their characteristics may reflect

different geological processes they have experienced, including partial melting and melt percolation. In particular, melt percolation events may have played a key role in generating the contrasting geochemical compositions between these two types. Below, we attempt to explain: (1) Why cpx in N-Type peridotites displays variable LREE enrichment and almost constant HREE, whereas cpx in E-Type peridotites shows enrichment of Fe, Ti and HREE (Figures 3 and 4). (2) Why IPGE in N-Type peridotites is high and homogenous, whereas that in E-Type peridotites is low and variable (Figure 6).

4.1 Variations of major and trace element compositions of Yong'an peridotites during mantle depletion and metasomatism

The Yong'an peridotites delineate a compositional spectrum from cpx-poor lherzolite to highly refractory harzburgite. In Figure 5, Al_2O_3 and CaO are negatively correlated with MgO, indicating that this spectrum can be interpreted as residues of variable degrees of partial melting [42, 45]. Specifically, N-Type peridotites show a large variation of $Cr^{\#}$(sp) (13.2–48), indicating moderate to high degrees of partial melting, whereas E-Type peridotites display high and restricted $Cr^{\#}$(sp) (35.3–42.2), corresponding to relatively high degrees of partial melting. Mantle residue after moderate to high degrees of partial melting are expected to be highly depleted in LILE, Fe and Ti, as demonstrated by the depleted abyssal peridotites [36]. However, all Yong'an peridotites are more enriched in LILE than the depleted abyssal peridotites (Figure 4(b) and (d)), and Ti and Fe enrichments in E-Type peridotites (Figure 3) are inconsistent with a partial melting trend. A reasonable interpretation is that the mantle domain represented by the Yong'an xenoliths has been modified by melt-rock reaction after the main partial melting event.

Two forms of interaction between melts and lithospheric mantle have been proposed to interpret the geochemical characteristics of peridotites, including ''wall-rock" metasomatism and cryptic metasomatism. ''Wall-rock" metasomatism is related to melt transport in fractures, forming veins and dykes, and is considered a local phenomenon. The metasomatic agent involved is generally a large melt fraction. Compositional and textural changes due to interaction with melts from fractures are generally confined to wall-rocks [54]. Wall-rock peridotites adjacent to veins are generally characterized by convex-upward or flat REE patterns, and Fe-enrichment. Cryptic metasomatism corresponds to melt migration by percolation along grain boundaries in a solid matrix (i.e., porous flow). The metasomatic agent involved is generally a small, volatile-rich melt fraction. Cryptic metasomatism is generally characterized by a lack of Fe-enrichment, and highly fractionated REE patterns ranging from U-shaped to steadily LREE-enriched patterns [55–57]. It is now widely accepted that selective enrichment of incompatible elements in many peridotites can be accounted for by chromatographic processes, such as proposed by Navon and Stolper [58].

N-Type peridotites display chondrite-normalized REE patterns of cpx marked by selective enrichment of LREE relative to HREE and or MREE ($(La/Yb)_n$ = 1.2–11.2), without significant Fe and Ti enrichment. In addition, there is no evidence for metasomatism-induced petrographic change. Therefore, the metasomatism responsible for the enrichment of incompatible elements in cpx of N-Type peridotites is largely cryptic. Lack of Fe and Ti enrichment is not consistent with wall-rock metasomatism. Instead, extremely variable LREE enrichment and almost constant HREE observed in cpx in N-Type peridotites (Figure 4) are virtually the same as those predicted by the Navon and Stolper's [58] chromatographic model. Cryptic metasomatism involving small melt fractions has also been invoked to explain the origin of the Shuangliao and Jiaohe peridotites from NE China [46]. Alternatively, LILE enrichment combined with HFSE depletion in cpx of N-Type peridotites may be related to metasomatism by evolved asthenosphere-derived melt, ephemeral carbonatite melts, or aqueous fluids [56, 59, 60].

The E-Type peridotites are mainly refractory harzburgites that display significant Fe and Ti enrichment in whole rocks, olivine, clinopyroxene and spinel (Figures 3 and 5). Similar characteristics have been observed in Huinan harzburgites, and considered to be products of melt-rock reaction during lithospheric thinning [61]. The E-Type peridotites do not display the strong LILE enrichment as present in the N-Type peridotites, and cpx separated from E-Type peridotites has nearly flat REE patterns (Figure 4(c)). The enrichment of Fe, Ti and HREE is consistent with "wall-rock" metasomatism involving high fractions of basaltic melts [61, 62]. This process commonly produces secondary recrystallization textures [56, 61, 63], but such textures are absent in the Yong'an peridotites.

4.2 Redistribution of PGE during mantle melting and metasomatism

It has been demonstrated that PGE in mantle peridotites is generally hosted mainly in base metal sulfides (Cu-Fe-Ni monosulfide solid solution (Mss), pentlandite and Cu-rich sulfides) [64–68]. The observed PGE systematics is controlled by the evolution of the sulfide component during mantle melting and melt percolation [49, 51, 69, 70]. For Yong'an peridotites, Al_2O_3 and Pd are positively correlated with sulfur contents (Figure 7(a) and (d)), indicating that sulfide and Pd are controlled mainly by partial melting. In contrast, there is no correlation between Ir, Os and sulfur (Figure 7(b) and (c)), which suggests that IPGE is not controlled mainly by sulfides. The whole rock Os and Ir concentrations, and ratios such as Os/Ir, of Yong'an xenoliths show a broad positive correlation with $(La/Sm)_n$ in cpx

(Figure 8(a)–(c)). Obviously, these correlations cannot be explained by partial melting process, but may be related to mantle metasomatism.

N-Type peridotites display a large range of sulfur contents (from 171 ppm to below detection limit, Table 4), constant IPGE contents and variable PPGE contents. Specifically, two N-Type peridotites (YA-2, YA-9) have high sulfur contents and relatively flat PGE patterns, indicating low degrees of melting [48, 64]. Other N-Type peridotites (YA-5, YA-8) have flat IPGE patterns but are depleted in PPGE relative to IPGE (Figure 6(a)) and correspond to moderate to high degrees of melting [10, 48, 51–53]. During low to moderate degree of partial melting (<10%), primary sulfides in N-Type peridotites were not exhausted (e.g., YA-2, YA-9, Table 4), and residual sulfides buffer PGE abundances to relatively constant levels because of the high $D_{sulfide/melt}$ (e.g., Lorand et al. [48]). When the degree of melting is higher (10%–22%), most primary sulfides dis-

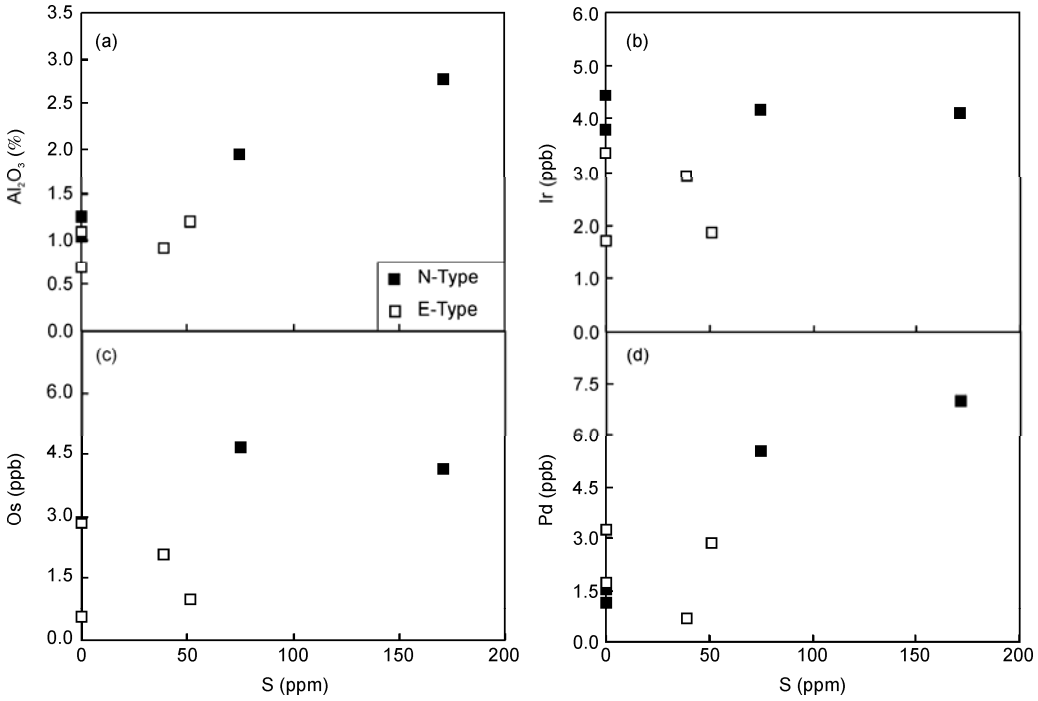

Figure 7 Plots of Al_2O_3, Ir, Os and Pd against sulfur for Yong'an peridotites.

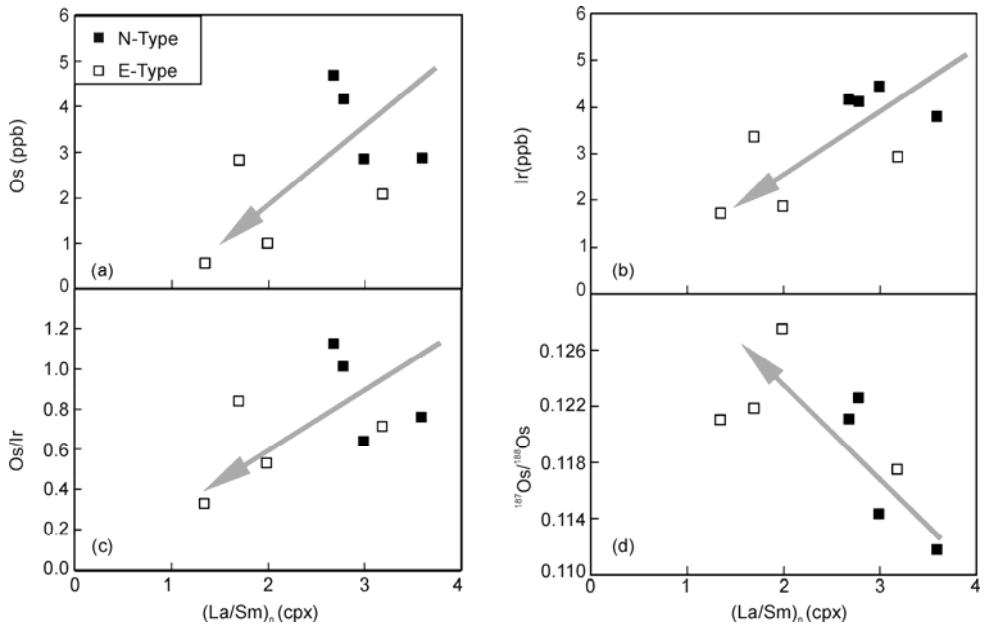

Figure 8 Plots of Os, Ir, Os/Ir and $^{187}Os/^{188}Os$ against $(La/Sm)_n$ in clinopyroxenes from Yong'an peridotites.

solve in basaltic melts (e.g., YA-5, YA-8, Table 4), and correspondingly, Pt and Pd abundances of peridotites sharply decrease. In contrast, IPGE may be hosted by other phases (such as spinel, laurite, Os-Ir-Ru alloys) rather than sulfides, and thus are immune to modification during partial melting events; they thus maintain relatively constant abundances [71, 72].

Although N-Type peridotites have suffered cryptic metasomatism by small melt fractions, as discussed in section 4.1, their PGE abundances appear to be unaffected by this process. As demonstrated in the deformed peridotites from Sidamo [10], infiltration of volatile-rich, small melt fractions significantly enhances Pd and to, a lesser extent, Rh, abundances by precipitating Cu-Ni rich sulfides along with metasomatic diopside. Metasomatic diopsides, olivines, and related silicate glasses are also observed in N-Type peridotites (e.g., YA-5, Figure 2(b)), although no sulfide grains or veins are present adjacent to these phases. This suggests that metasomatism of N-Type peridotites involving small melt fractions did not introduce secondary Cu-Pd rich sulfides. This assumption is further supported by the positive correlation between Al_2O_3 and Pd contents (Figure 9).

In contrast, E-Type peridotites display overall low sulfur and PGE abundances (Table 4, Figure 6(b)), with low and variable IPGE contents (Figure 9). Low contents of sulfur and PPGE in E-Type peridotites are consistent with relatively high degrees of melting, as discussed in section 4.1. However, sub-chondritic and variable IPGE contents cannot be explained by melt depletion events, because Os, Ir, and Ru abundances are expected to stay relatively constant or even increase during partial melting [51, 52]. Furthermore, mantle peridotites and ultramafic melts contain IPGE in generally chondritic abundances, implying that these elements are not significantly fractionated during partial melting [69, 75]. Sulfide breakdown during weathering is also excluded, because all Yong'an peridotites are fresh (LOI <0.3%).

A more widely invoked interpretation might be dissolution of primary sulfides during wall-rock metasomatism at high melt-rock ratios, as proposed in previous studies [7, 9, 10, 66, 76]. In this process, original sulfides, as the main PGE-bearing phase, were removed along with percolating melts, resulting in a decrease of sulfur contents and Os, Ir, Ru depletion. This assumption is attractive, because significant Fe-Ti enrichment and nearly flat REE patterns of E-Type peridotites are consistent with wall-rock metasomatism at high melt-rock ratios (Figures 3, 5(c)). However, this model appears to be inapplicable for the Yong'an case given the following considerations:

(1) This interpretation predicts a positive correlation between sulfur contents and IPGE abundances, but this correlation is absent in E-Type peridotites.

(2) This model predicts that the removal of primary sulfides during melt percolation would decrease abundances of Os, Ir, Ru, but would not result in fractionation of these IPGE. However, E-Type peridotites show a large variation of Os/Ir and Ru/Ir ratios (Os/Ir = 0.33–0.84, Ru/Ir = 0.94–1.6; Table 4). Some are characterized by negative Os and Ru anomalies relative to Ir (YA-6, YA-7, Figure 6(b)).

(3) It is expected that Pt and Pd contents are more sensitive to melt percolation than IPGE, because these elements are confined to sulfides, whereas IPGE are only partly held in sulfides. Thus, removal of sulfides during melt-rock reaction will more severely modify Pt and Pd rather than Os, Ir

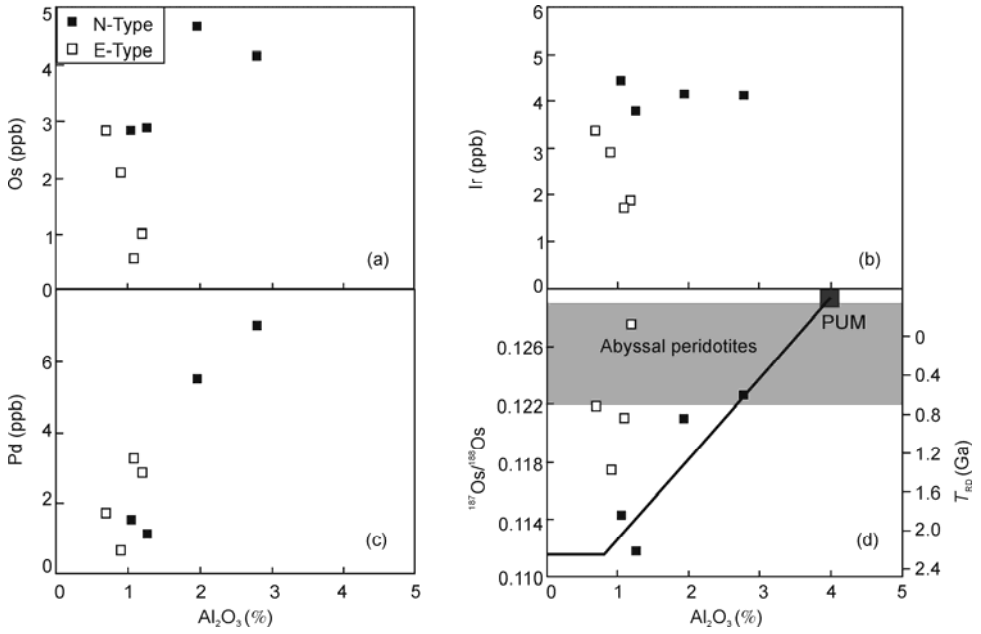

Figure 9 Correlations of HSE contents and $^{187}Os/^{188}Os$ ratios versus bulk Al_2O_3 contents. Shaded area in (d) represents average Os isotope compositions of abyssal peridotites [73]. PUM represents Primitive upper Mantle [74].

and Ru contents. However, the positive correlation between Pd and Al_2O_3 contents in Yong'an peridotites (Figure 9(c)) indicates that Pd contents in Yong'an peridotites are controlled mainly by partial melting events rather than melt percolation. Therefore sulfide transfer during melt-rock reaction cannot account for both the IPGE and PPGE contents of these peridoitites.

As discussed above, PGE compositions of E-Type peridotites cannot be explained by dissolution of primary sulfides during wall-rock metasomatism at high melt-rock ratios. Therefore, a new model is needed to account for (1) the sub-chondritic IPGE pattern of E-Type peridotites (Figure 6(b)); (2) the fractionation of IPGE in E-Type peridotites compared to primitive mantle (Table 4); and (3) the apparently unmodified Pd contents of E-Type peridotites after the partial melting event that produced these residues, as illustrated by the positive correlation of Pd with Al_2O_3 contents (Figure 9(c)).

At high degrees of melting, most sulfides are dissolved in the silicate melts. Sulfur abundance decreases, and the abundances of PPGE, mainly hosted by sulfides, are significantly lowered. In contrast, discrete microphases such as Ru-Os-(Ir) alloys or laurite, as inclusions in mantle chromites, are more likely in the context of low $f\,S_2$ generated by high degree melting [71, 77, 78]. Therefore, IPGE hosted by laurite and/or Os-Ir-Ru alloys will remain in the residual peridotites. Given these metal phases in peridotites were removed during later metasomatism, correspondingly, IPGE contents of peridotites will be significantly modified. We argue that Os, Ir and Ru depletion of the studied E-Type peridotites is a product of removal of metallic phases, such as laurite or Os-Ir-Ru alloy during wall-rock metasomatism at high melt-rock ratios. In particular, removal of laurite $(Ru,Os)S_2$ during metasomatism at high melt-rock ratios can explain inter-elemental IPGE fractionation in E-Type peridotites (as illustrated by variable Os/Ir and Ru/Ir, Table 4). As these phases are quite rare and usually very small, they are highly unlikely to be detected during routine petrographic inspection of a restricted number of polished thin sections [10]. In addition, removal of metallic phases during wall-rock metasomatism is not accompanied by significant secondary sulfides infiltration from the invading melt, so Pd and sulfur contents of E-Type peridotites remain positively correlated with Al_2O_3 (Figures 7(a), 9(c)).

4.3 Evolution of Re-Os isotopic systematics during partial melting and melt-rock interaction

The Re-Os system has proven to be useful in dating melt depletion events in peridotites, and in the last two decades, it has been widely used to constrain the timing of melt extraction events in mantle peridotites and associated sulfides [2, 3, 12, 79–81]. During mantle melting, Re behaves as a mildly incompatible element, whereas Os behaves as a compatible element [1, 2]. After radiogenic decay, positive trends are expected to be formed on Al_2O_3 versus $^{187}Os/^{188}Os$ plots [74]. However, $^{187}Os/^{188}Os$ and Os model ages can be altered during melt-rock reaction, as reported for some mantle wedge peridotites and peridotite massifs [5, 7–9].

Yong'an peridotites display a large range of $^{187}Os/^{188}Os$ at comparable levels of fertility (0.11179–0.12752). The $^{187}Re/^{188}Os$ ratios for all samples do not correlate with their $^{187}Os/^{188}Os$ ratios. This lack of correlation is common and may be attributable to several factors, including derivation of samples from isotopically distinct portions of the SCLM, and late-stage Re mobility [6, 74]. A negative correlation exists between whole rock $^{187}Os/^{188}Os$ ratios and $(La/Sm)_n$ in Cpx (Figure 8(d)), which indicates that melt percolation played an important role in Re-Os isotopic systematics.

N-Type peridotites display high and a restricted range of Os concentrations (2.85–4.68 ppb) and a positive correlation between $^{187}Os/^{188}Os$ and Al_2O_3, which can be explained by radiogenic decay after mantle depletion events. Sample YA-5 has an $^{187}Os/^{188}Os$ ratio of 0.11179, which is among the lowest values measured so far for the mantle xenoliths in the Hinggan-Mongolian Orogenic Belt [4, 82]. Although N-Type peridotites have suffered cryptic metasomatism by small melt fractions (Section 4.1), their Os isotope compositions seem to be immune to this process.

E-Type peridotites show overall lower Os contents, higher $^{187}Os/^{188}Os$ ratios and younger T_{RD} model ages (mostly <1 Ga) than those of N-Type peridotites at comparable fertility levels (Figures 6(b) and 9(d)). Low Os contents in E-Type peridotites can be explained by removal of microphases containing IPGE, such as Ru-Os-(Ir) alloys or laurite, during extensive melt-rock reaction (see discussion above). $^{187}Os/^{188}Os$ ratios of E-Type peridotites are higher than those of N-Type peridotites at comparable fertility levels (Figure 9(d)). Some samples of E-Type peridotites plot within, or close to, the abyssal peridotite field. Similar features were observed in peridotites from Qixia, Shuangliao and Wangqing, in eastern China, and were considered to be newly formed lithospheric mantle after young melt depletion events (<1 Ga) [4, 12]. In contrast, we favor that the $^{187}Os/^{188}Os$ ratios of E-Type peridotites from Yong'an are elevated during extensive melt-rock reaction rather than representing new formed lithospheric mantle for the following reasons: (1) E-Type peridotites deviate from the common "depletion trend"; in terms of both whole rock and mineral compositions; these samples are characterized by relatively higher contents of TiO_2 and FeO in constituent minerals and incompatible elements (REE and LILE) in cpx compared to the depletion trend (Figures 3, 4), as a result of melt-percolation. (2) The negative correlation between whole rock $^{187}Os/^{188}Os$ and cpx $(La/Sm)_n$ (Figure 8(d)) is considered to be evidence of mantle metasomatism rather than reflecting partial melting events. To sum up, although N-Type peridotites have suffered cryptic metasomatism by small melt fractions, their Os isotope compositions appear

unaffected by this process. The overall low Os contents and radiogenic Os isotope compositions of E-Type peridotites may be explained by removal of Os-bearing microphases, such as Ru-Os-(Ir) alloys or laurite, followed by precipitation from melt of secondary sulfides with radiogenic isotopic signatures during extensive melt-rock reaction.

4.4 Implications for the age of SCLM beneath the Hinggan-Mongolian Orogenic Belt

The Re-depletion ages (T_{RD}) for the Yong'an samples (except for YA-6), assuming a Re/Os of zero [2], range from 0.65 to 2.23 Ga (Table 4). Because Re contents in peridotites are certainly higher than zero after melt extraction, T_{RD} may underestimate the true ages of melting events and is considered as minimum model ages [2]. Only the Re depletion age of the most refractory samples may approach that of the true age. Moreover, metasomatic enrichment tends to be involved to a greater degree in more refractory samples [19, 34]. In this sense, 2.23 Ga may represent the age of melt extraction although this is still a minimum estimate given the presence of more refractory samples.

Peridotites in NE China are characterized by a wide range of $^{187}Os/^{188}Os$ at comparable Al_2O_3 contents, and show a very poor correlation between $^{187}Os/^{188}Os$ ratio and Al_2O_3 content (Figure 10(a)), features also reported from peridotite xenoliths from the eastern North China Craton [4, 12, 13]. The poor correlation between $^{187}Os/^{188}Os$ and Al_2O_3 content has been explained by both Proterozoic and Phanerozoic additions to the SCLM underlying the HMOB during several partial melting events [4]. However, redistribution of Os-bearing minerals during melt-rock reaction also can elevate $^{187}Os/^{188}Os$ and disrupt the correlation between $^{187}Os/^{188}Os$ and Al_2O_3, as demonstrated in the Yong'an peridotites. Due to a lack of PGE and sulfur data in previous study of peridotites from Shuangliao, Wangqing, Jiaohe, NE China [4, 82], it is hard to evaluate the effect of melt-rock reaction on PGE and Re-Os systematic of these peridotites. We note that there is a negative correlation between Os and $^{187}Os/^{188}Os$ (Figure 10(b)), which cannot be explained by partial melting, but may be related to melt-rock reaction.

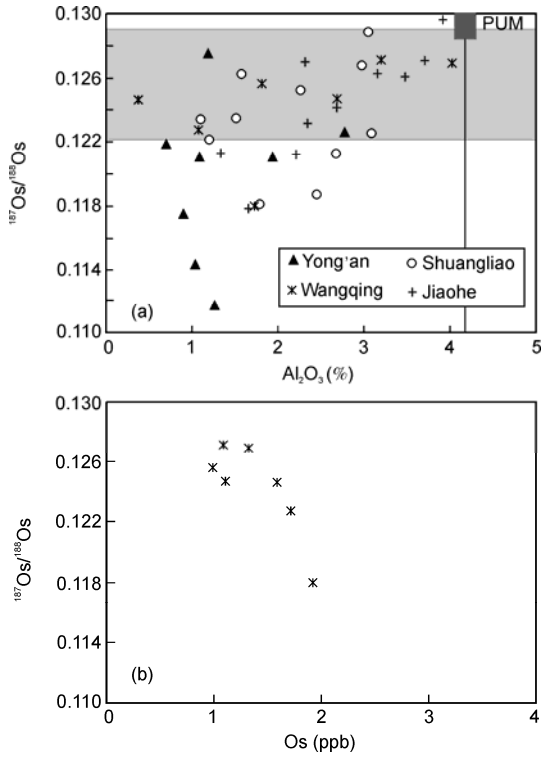

Figure 10 $^{187}Os/^{188}Os$ versus Al_2O_3 content for peridotites from NE China (a) and $^{187}Os/^{188}Os$ versus Os content of peridotites from Wangqing (b). Os isotope data of peridotites in NE China are from refs. [4, 82] and this study.

5 Conclusions

Yong'an peridotite xenoliths range from relatively fertile lherzolite to refractory harzburgites, which are divided into two groups: N-Type and E-type. The N-Type group including cpx-poor lherzolite and harzburgite shows a large variation of $Cr^{\#}$(sp) (13.2–48), indicating moderate to high degrees of partial melting, whereas the E-Type peridotites are mainly refractory harzburgites, and characterized by high $Cr^{\#}$(sp) (35.3–42.2), corresponding to relatively high degrees of partial melting. Compared to N-Type, E-Type displays significant Fe and Ti enrichment in both whole rock and separated minerals. Furthermore, the N-Type peridotites display a restricted range of Os/Ir and Ru/Ir ratios (Os/Ir = 0.64–1.12, Ru/Ir = 1.52–1.79), whereas the E-Type peridotites show a large variation of Os/Ir and Ru/Ir ratios (Os/Ir = 0.33–0.84, Ru/Ir = 0.94–1.60). $^{187}Os/^{188}Os$ ratios of E-Type peridotites are higher than those of N-Type peridotites at comparable fertility levels. These results suggest that N-Type peridotites may have been modified by metasomatism by small melt fractions, in which the percolation of the volatile-rich, small melt fractions may only result in LILE enrichment of clinopyroxene, while their whole rock PGE contents and Re-Os isotope values were little changed. Moreover, the E-Type peridotites may have been modified by extensive melt-rock reaction with large melt fractions, which may result in the removal of IPGE-bearing minerals such as Ru-Os-(Ir) alloys or laurite, followed by precipitation of secondary sulfides from melt with radiogenic isotopic signature.

The SCLM in NE China is essentially Proterozoic in age. The transport and redistribution of Os-bearing minerals during melt-rock reaction cannot be ignored in generating the elevated $^{187}Os/^{188}Os$ ratios in peridotites and "young" lithosphere in NE China.

The authors would like to thank Lu Xiaoping, Qin Xiufeng and Nie Xiaoyong for their support during the fieldwork, Hu Jing, Huang Yan and Deng Yufeng for their technical help with trace element and PGE analyses. Reviews by Zhang Hongfu and an anonymous referee greatly improved this

paper. This study was supported by National Natural Science Foundation of China (Grant Nos. 40903019, 40730420, 70914001), project of "CAS Hundred Talents", project of Chinese Academy of Sciences (Grant No. KZCX2-YW-Q04-06) and special project of State Key Laboratory of Ore Deposit Geochemistry (Grant No. KCZX20090105).

1 Morgan J M. Ultramafic xenoliths: Clues to Earth's late accretionary history. J Geophys Res, 1986, 91: 12375–12387
2 Walker R J, Carlson R W, Shirey S B, et al. Os, Sr, Nd, and Pb isotope systematics of southern African peridotite xenoliths: Implications for the chemical evolution of the subcontinental mantle. Geochim Cosmochem Acta, 1989, 53: 1583–1595
3 Reisberg L, Lorand J P. Longevity of sub-continental mantle lithosphere from osmium isotope systematics in orogenic peridotite massifs. Nature, 1995, 376: 159–162
4 Wu F Y, Walker R J, Ren X W, et al. Osmium isotopic constraints on the age of lithospheric mantle beneath northeastern China. Chem Geol, 2003, 196: 107–129
5 Brandon A D, Creaser R A, Shirey S B, et al. Osmium recycling in subduction zones. Science, 1996, 272: 861–864
6 Chesley J T, Rudnick R L, Lee C T. Re-Os systematics of mantle xenoliths from the East African Rift: Age, structure, and history of the Tanzanian craton. Geochim Cosmochem Acta, 1999, 63: 1203–1217
7 Becker H, Shirey S B, Carlson R W. Effects of melt percolation on the Re-Os systematics of peridotites from a Paleozoic convergent plate margin. Earth Planet Sci Lett, 2001, 188: 107–121
8 Büchl A, Brügmann G, Batanova V G, et al. Melt percolation monitored by Os isotopes and HSE abundances: A case study from the mantle section of the Troodos Ophiolite. Earth Planet Sci Lett, 2002, 204: 385–402
9 Büchl A, Brügmann G E, Batanova V G, et al. Os mobilization during melt percolation: The evolution of Os isotope heterogeneities in the mantle sequence of the troodos ophiolite, Cyprus. Geochim Cosmochem Acta, 2004, 68: 3397–3408
10 Lorand J P, Reisberg L, Bedini R M. Platinum-group elements and melt percolation processes in Sidamo spinel peridotite xenoliths, Ethiopia, East African Rift. Chem Geol, 2003, 196: 57–75
11 Lorand J P, Delpech G, Grégoire M, et al. Platinum-group elements and the multistage metasomatic history of Kerguelen lithospheric mantle (South Indian Ocean). Chem Geol, 2004, 208: 195–215
12 Gao S, Rudnick R L, Carlson R W, et al. Re-Os evidence for replacement of ancient mantle lithosphere beneath the North China craton. Earth Planet Sci Lett, 2002, 198: 307–322
13 Wu F Y, Walker R J, Yang Y H, et al. The chemical-temporal evolution of lithospheric mantle underlying the North China Craton. Geochim Cosmochem Acta, 2006, 70: 5013–5034
14 Zhang H F, Goldstein S L, Zhou X H, et al. Comprehensive refertilization of lithospheric mantle beneath the North China Craton: Further Os-Sr-Nd isotopic constraints. J Geol Soc, 2009, 166: 249–259
15 Reisberg L, Zhi X, Lorand J P, et al. Re-Os and S systematics of spinel peridotite xenoliths from east central China: Evidence for contrasting effects of melt percolation. Earth Planet Sci Lett, 2005, 239: 286–308
16 Jahn B M, Wu F Y, Chen B. Massive granitoids generation in Central Asia: Nd isotope evidence and implication for continental growth in the Phanerozoic. Episodes, 2000, 23: 82–92
17 Liu R X. The Age and Geochemistry of Cenozoic Volcanic Rocks in China (in Chinese). Beijing: Seismological Press, 1992
18 Qin X F, Xu Y G, Zhang H H, et al. Petrogenetic diversity of continental subalkaline volcanic rocks: An example from the Dunhua-Mishan-Dongning volcanic belt (in Chinese). Acta Petrlo Sin, 2008, 24: 2501–2514
19 Frey F A, Prinz M. Ultramafic inclusions from San Carlos, Arizona: Petrologic and geochemical data bearing on their petrogenesis. Earth Planet Sci Lett, 1978, 38: 129–176
20 Yu S Y, Xu Y G, Huang X L, et al. Characteristics of melt-rock reaction in Shuangliao peridotite xenoliths and their implications to mantle metasomatism (in Chinese). Acta Petrolo Min, 2007, 26: 213–222
21 Qi L, Hu J, Conrad G. Determination of trace elements in granites by inductively coupled plasma ass spectrometry. Talanta, 2000, 51: 507–513
22 Qi L, Zhou M F, Wang C Y. Determination of low concentrations of platinum group elements in geological samples by ID-ICP-MS. J Anal At Spectrom, 2004, 19: 1335–1339
23 Meisel T, Moser J. Reference materials for geochemical PGE analysis: New analytical data for Ru, Rh, Pd, Os, Ir, Pt and Re by isotope dilution ICP-MS in 11 geological reference materials. Chem Geol, 2004, 208: 319–338
24 Govindaraju K. Complication of working values and sample descriptions for 383 geostandards. Geostand Geoanal Res, 1994, 18: 1–55
25 Shirey S B, Walker R J. Carius tube digestion for low blank rhenium-osmium analyses. Anal Chem, 1995, 34: 2136–2141
26 Cohen A S, Waters F G. Separation of osmium from geological materials by solvent extraction for analysis by thermal ionization mass spectrometry. Anal Chim Acta, 1996, 332: 269–275
27 Pearson D G, Woodland S J. Solvent extraction/anion exchange separation and determination of PGEs (Os, Ir, Pt, Pd, Ru) and Re-Os isotopes in geological samples by isotope dilution ICP-MS. Chem Geol, 2000, 165: 87–107
28 Li J, Liang X R, Dong Y H, et al. Measurements of Re-Os isotopic compositions in mafic-ultramafic rocks by multi-collector inductively coupled plasma mass spectrometer (MC-ICPMS) (in Chinese). Geochimica, 2007, 36: 153–160
29 Roy-Barman M, Luck J M, Allégre C J. Os isotopes in orogenic lherzolite massifs and mantle heterogeneities. Chem Geol, 1996, 130: 55–64
30 Creaser R A. Papanastassiou D A, Wasserburg G J. Negative thermal ion mass spectrometry of osmium, rhenium and iridium. Geochim Cosmochem Acta, 1991, 55: 397–401
31 Volkening J, Walczyk T G, Heumann K. Osmium isotope ratio determinations by negative thermal ionization mass spectrometry. Int J Mass Spectr Ion Proc, 1991, 105: 147–159
32 Nier A O. The isotopic constitution of osmium. Phys Rev, 1937, 52: 885–892
33 Bédard L P, Savard D, Barnes S J. Total sulfur concentration in geological reference materials by elemental infrared analyzer. Geostand Geoanal Res, 2008, 32: 203–208
34 Xu Y G, Menzies M A, Vroon P, et al. Texture-temperature-geochemistry relationships in the upper mantle as revealed from Spinel Peridotite xenoliths from Wangqing, NE China. J Petrol, 1998, 39: 469–493
35 Dick J B, Bullen T. Chromian spinel as a petrogenetic indicator in abyssal and alpine-type peridotites and spatially associated lavas. Contrib Mineral Petrol, 1984, 86: 54–76
36 Johnson K T M, Dick H J B, Shimizu N. Melting in the oceanic upper mantle: an ion microprobe study of diopsides in abyssal peridotites. J Geophys Res, 1990, 95: 2661–3267
37 Bertrand P, Mercier J C. The mutual solubility of coexisting ortho- and clinopyroxene: Toward an absolute geothermometer for the natural system? Earth Planet Sci Lett, 1985, 76: 109–122
38 Wells R A. Pyroxene thermometry in simple and complex systems. Contrib Mineral Petrol, 1977, 62: 129–139
39 Witt-Eickschen G, Seck H A. Solubility of Ca and Al in orthopyroxene from spinel peridotite: An improved version of an empirical geothermometer. Contrib Mineral Petrol, 1991, 106: 431–439
40 Shirey S B, Walker R J. The Re-Os isotope system in cosmochemistry and hightemperature geochemistry. An Rev Earth Planet Sci, 1998, 26: 423–500
41 Sun S S, McDonough W F. Chemical and isotopic systematics of oceanic basalts: implications for mantle composition and processes. Geol Soc Spec Pub, 1989, 42: 313–345
42 Takazawa E, Frey F A, Shimizu N, et al. Whole rock compositional variations in an upper mantle peridotite (Horoman, Hokkaido, Japan): Are they consistent with a partial melting process? Geochim Cosmochem Acta, 2000, 64: 695–716
43 Niu Y L. Mantle melting and melt extraction processes beneath ocean ridges: Evidence from abyssal peridotites. J Petrol, 1997, 38: 1047–

1074
44 Hart S R, Zindler A. In search of a bulk Earth composition. Chem Geol, 1986, 57: 247–267
45 Frey F A, Suen C J, Stockman H W. The Ronda high temperature peridotite: Geochemistry and petrogenesis. Geochim Cosmochem Acta, 1985, 49: 2469–2491
46 Yu S Y, Xu Y G, Huang X L, et al. Hf-Nd isotopic decoupling in continental mantle lithosphere beneath Northeast China: Effects of pervasive mantle metasomatism. J Asian Earth Sci, 2009, 35: 554–570
47 McDonough W F, Sun S S. The composition of the Earth. Chem Geol, 1995, 120: 223–253
48 Lorand J P, Pattou L, Gros M. Fractionation of platinum-group elements and gold in the upper mantle: A detailed study in Pyrenean orogenic lherzolites. J Petrol, 1999, 40: 957–981
49 Becker H, Horan M F, Walker R J, et al. Highly siderophile element composition of the Earth's primitive upper mantle: Constraints from new data on peridotite massifs and xenoliths. Geochim Cosmochem Acta, 2006, 70: 4528–4550
50 Anders E, Grevesse N. Abundances of the elements: meteoritic and solar. Geochim Cosmochem Acta, 1989, 53: 197–214
51 Pearson D G, Irvine G J, Ionov D A, et al. Re-Os isotope systematics and platinum group element fractionation during mantle melt extraction: A study of massif and xenolith peridotite suites. Chem Geol, 2004, 208: 29–59
52 Batanova V G, Brügmann G E, Bazylev B A, et al. Platinum-group element abundances and Os isotope composition of mantle peridotites from the Mamonia complex, Cyprus. Chem Geol, 2008, 248: 195–212
53 Gueddari K, Piboule M, Amoss J. Differentiation of platinum-group elements (PGE) and of gold during partial melting of peridotites in the lherzolitic massifs of the Betico-Rifean range (Ronda and Beni Bousera). Chem Geol, 1996, 134: 181–197
54 Kempton P D. Mineralogic and geochemical evidence for differing styles of metasomatism in spinel lherzolite xenoliths: Enriched mantle source regions of basalts? In: Menzies M, Hawkesworth C J, eds. Mantle Metasomatism. New York: Academic Press, 1987
55 Bodinier J L, Vasseur G, Vernieres J, et al. Mechanisms of mantle metasomatism: Geochemical evidence from the Lherz Orogenic peridotite. J Petrol, 1990, 31: 597–628
56 Bedini R M, Bodinier J L, Dautria J M, et al. Evolution of LILE-enriched small melt fractions in the lithospheric mantle: A case study from the East African Rift. Earth Planet Sci Lett, 1997, 153: 67–83
57 Ionov D A, Harmer R E. Trace element distribution in calcite-dolomite carbonatites from Spitskop: Inferences for differentiation of carbonatite magmas and the origin of carbonates in mantle xenoliths. Earth Planet Sci Lett, 2002, 198: 495–510
58 Navon O, Stolper E. Geochemical consequence of melt percolation: The upper mantle as a chromatographic column. J Geol, 1987, 95: 285–307
59 McKenzie D P. Some remarks on the movement of small melt fractions in the mantle. Earth Planet Sci Lett, 1989, 95: 53–72
60 Ionov D A, Dupuy C, O'Reilly S Y, et al. Carbonated peridotite xenoliths from Spitsbergen: Implications for trace element signature of mantle carbonate metasomatism. Earth Planet Sci Lett, 1993, 119: 283–297
61 Xu Y G, Menzies M A, Thirlwall M F, et al. "Reactive" harzburgites from Huinan, NE China: Products of the lithosphere-asthenosphere interaction during lithospheric thinning? Geochim Cosmochem Acta, 2003, 67: 487–505
62 Edwards S J, Malpas J. Melt-peridotite interactions in shallow mantle at the East Pacific Rise: Evidence from ODP site 895 (Hess Deep). Mineral Mag, 1996, 60: 191–206
63 Godard M, Bodinier J L, Vasseur G. Effects of mineralogical reaction on trace element redistributions in mantle rocks during percolation processes: A chromatographic approach. Earth Planet Sci Lett, 1995, 133: 449–461
64 Handler M R, Bennett V C. Behavior of Platinum-group elements in the subcontinental mantle of eastern Australia during variable metasomatism and melt depletion. Geochim Cosmochem Acta, 1999, 63: 3597–3618
65 Alard O, Griffin W L, Lorand J P, et al. Non-chondritic distribution of the highly siderophile elements in mantle sulphides. Nature, 2000, 407: 891–894
66 Lorand J P, Alard O. Platinum-group element abundances in the upper mantle: New constraints from *in situ* and whole-rock analyses of Massif Central xenoliths (France). Geochim Cosmochem Acta, 2001, 65: 2789–2806
67 Luguet A, Alard O, Lorand J P, et al. Laser-ablation microprobe (LAM)-ICPMS unravels the highly siderophile element geochemistry of the oceanic mantle. Earth Planet Sci Lett, 2001, 189: 285–294
68 Luguet A, Lorand J P, Seyler M. Sulfide petrology and highly siderophile element geochemistry of abyssal peridotites: A coupled study of samples from the Kane Fracture Zone (45°W, 23°20′N, MARK area, Atlantic Ocean). Geochim Cosmochem Acta, 2003, 67: 1553–1570
69 Rehkämper M, Halliday A N, Alt J, et al. Non-chondritic platinum-group element ratios in oceanic mantle lithosphere: Petrogenetic signature of melt percolation? Earth Planet Sci Lett, 1999, 172: 65–81
70 Rudnick R L, Walker R J. Interpreting ages from Re-Os isotopes in peridotites. Lithos, 2009, 112: 1083–1095
71 Brenan J M, Andrews D. High-temperature stability of laurite and Ru-Os-Ir alloy and their role in PGE fractionation in mafic magmas. Can Mineral, 2001, 39: 341–360
72 Righter K, Campbell A J, Humayun M, et al. Partitioning of Ru, Rh, Pd, Re, Ir, and Au between Cr-bearing spinel, olivine, pyroxene and silicate melts. Geochim Cosmochem Acta, 2004, 68: 867–880
73 Snow J E, Reisberg L. Os isotopic systematics of the MORB mantle: Results from altered abyssal peridotites. Earth Planet Sci Lett, 1995, 136: 723–733
74 Meisel T, Walker R J, Irving A J, et al. Osmium isotopic compositions of mantle xenoliths: A global perspective. Geochim Cosmochem Acta, 2001, 65: 1311–1323
75 Lorand J P, Schmidt G, Palme H, et al. Highly siderophile element geochemistry of the Earth's mantle: New data for the Lanzo (Italy) and Ronda (Spain) orogenic peridotite bodies. Lithos, 2000, 53: 149–164
76 Reisberg L, Lorand J P, Bedini R M. Reliability of Os model ages in pervasively metasomatized continental mantle lithosphere: A case study of Sidamo spinel peridotite xenoliths (East African Rift, Ethiopia). Chem Geol, 2004, 208: 119–140
77 Ballhaus C. Is the upper mantle metal-saturated? Earth Planet Sci Lett, 1995, 132: 75–86
78 Rehkämper M, Halliday A N, Fitton J G, et al. Ir, Ru, Pt, and Pd in basalts and komatiites: New constraints for the geochemical behavior of the platinum-group elements in the mantle. Geochim Cosmochem Acta, 1999, 63: 3915–3934
79 Carlson R W, Irving A J. Depletion and enrichment history of subcontinental lithospheric mantle: An Os, Sr, Nd and Pb isotopic study of ultramafic xenoliths from the northwestern Wyoming Craton. Earth Planet Sci Lett, 1994, 126: 457–472
80 Aulbach S, Griffin W L, Pearson N J, et al. Mantle formation and evolution, Slave Craton: Constraints from HSE abundances and Re-Os isotope systematics of sulfide inclusions in mantle xenocrysts. Chem Geol, 2004, 208: 61–88
81 Xu Y G, Blusztajn J, Ma J L, et al. Late Archean to Early Proterozoic lithospheric mantle beneath the western North China Craton: Sr-Nd-Os isotopes of peridotite xenoliths from Yangyuan and Fansi. Lithos, 2008, 102: 25–42
82 Zhou Q, Wu F Y, Chu Z Y, et al. Sr-Nd-Hf-Os isotope characterizations of the Jiaohe peridotite xenoliths in Jilin Province and constraints on the lithospheric mantle age in northeastern China (in Chinese). Acta Petrol Sin, 2007, 23: 1269–1280